# Supplementary Materials

# UiO66-$NH_2$@$In_2O_3$ Heterostructures for Improved Photocatalytic $CO_2$ Reduction

Bolin Ma[1,#], Guanghui Chen[1,#], Lingling Zhou[1], Chengyang Ni[1], Xinyu Sun[1], Lei Zhang[1], Xinguo Xi[1], Lanqin Tang[1,2*], Yong Zhou[2*]

[1] Department of Chemistry and Chemical Engineering, Yancheng Institute of Technology, Yancheng, Jiangsu 224051, P. R. China

[2] School of Physics, Jiangsu Key Laboratory of Nanotechnology, Eco-materials and Renewable Energy Research Center (ERERC), National Laboratory of Solid State Microstructures, Collaborative Innovation Center of Advanced Microstructures, Nanjing University, Nanjing 210093, P. R. China

*Corresponding authors: lanqin_tang@163.com; zhouyong1999@nju.edu.cn

[#] These authors contributed equally.

**Table S1.** A brief survey of $CO_2$ reduction performances of reported photocatalysts.

| Samples | Sacrificial agent | Products | Productivity (μmol/g/h) | Ref. |
|---|---|---|---|---|
| UiO66-$NH_2$@$In_2O_3$ | $H_2O$ | CO | 69.30 | This work |
| Ag/GaOOH/$CaTiO_3$ | $H_2O$ | CO | 0.04 | 1 |
| UiO66 with Defects | $H_2O$ | CO | 1.33 | 2 |
| UiO68-$NH_2$-ML100 | TEOA | CO | 21.3 | 3 |
| Ni-MOF ($H_2O$) | $Ru(bpy)_3Cl_2 \cdot 6H_2O$ TEOA | CO | 9610 | 4 |
| Co-MOF/$Cu_2O$ | $H_2O$ | CO | 3.83 | 5 |
| PCN222-Cu@TpPa1 | $H_2O$ | CO<br>$CH_4$ | 0.6<br>21.3 | 6 |
| PCN-224(Cu)/$TiO_2$ | $H_2O$ | CO | 37.21 | 7 |


1. H.X. Qiu, A. Yamamoto, H. Yoshida, *Sustainable Energy Fuels*, 2024,8, 1287-1294.
2. Y.Q. He, C.G. Li, X.B. Chen, Z. Shi, S.H. Feng, *ACS Appl. Mater. Interfaces* 2022, 14, 25, 28977–28984.
3. S.Q. Wang, X.Z. Wang, X.M. Cheng, J. Ma, W.Y. Sun, *J. Mater. Chem. A*, 2022, 10, 16396-16402.
4. K.N. Song, S.J. Liang, X.H. Zhong, M.Y. Wang, X.F. Mo, X.Q. Lei, Z. Lin, *Applied Catalysis B: Environmental*, 2022, 309,121232.
5. W.W. Dong, J. Jia, Y. Wang, J.R. An, O.Y. Yang, X.J. Gao, Y.L. Liu, J. Zhao, D.S. Li, *Chem. Eng. J.*, 438, 2022,135622.
6. Z.L. Wu, W. Li, L.L. Hou, Q.M. Wei, H.X. Yang, Y.Y. Jiang, D.Y. Tang, *Sep. Purif. Technol.*, 311, 2023, 123322.
7. L. Wang, P.X. Jin, J.W. Huang, H.D. She, Q.Z. Wang, *ACS Sustain. Chem. Eng*, 18, 2019, 7, 15660-15670.

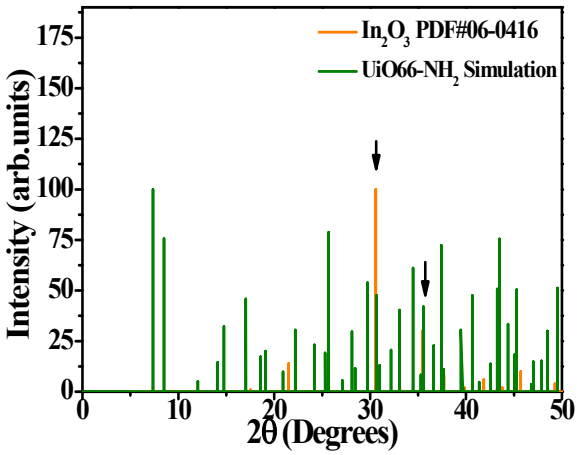


**Figure S1.** The standard XRD pattern of $In_2O_3$ and UiO66-$NH_2$ shows that the main $In_2O_3$ peaks around 30° and 35° overlap with the diffraction peaks of UiO66-$NH_2$, making it difficult to distinguish the $In_2O_3$ phase in the heterostructure.

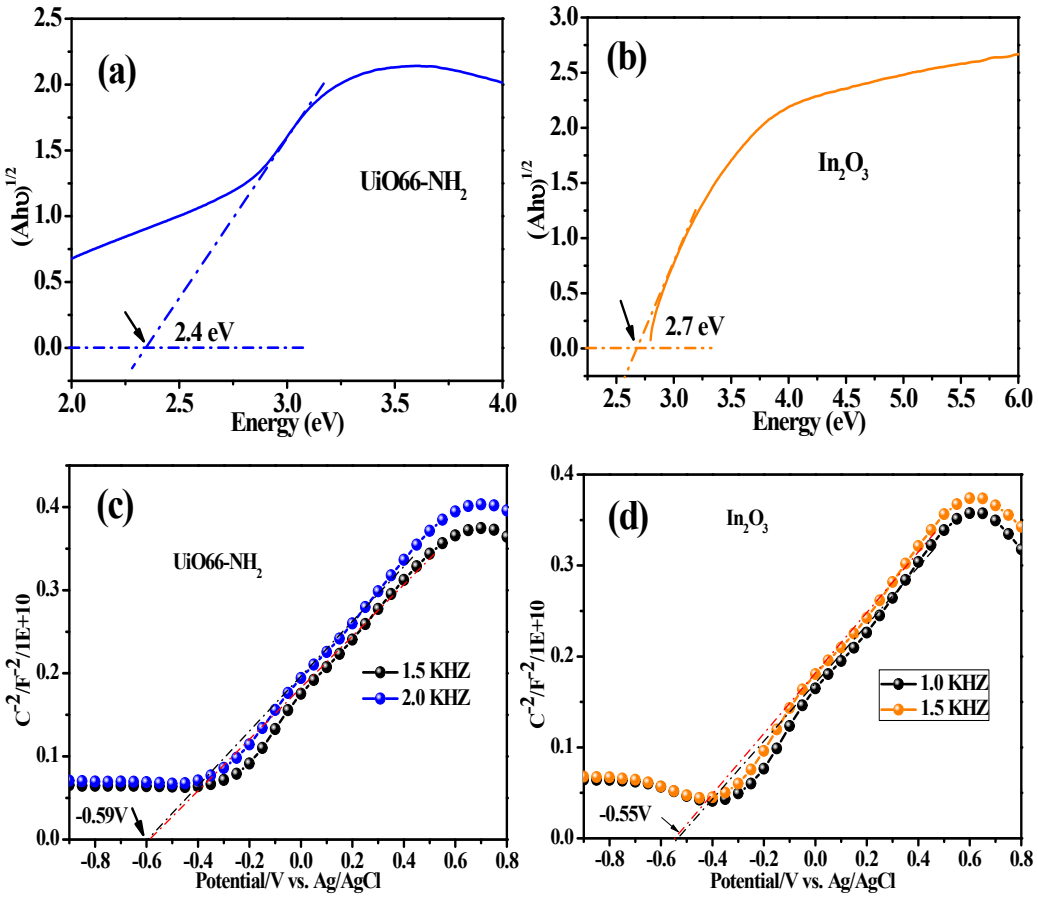


**Figure S2.** (a, b) The estimated band gap of UiO66-$NH_2$ and $In_2O_3$ from Tauc plots. (c, d) Mott-Schottky curves of samples tested at 1000 Hz and 1500Hz in 0.5 mol $L^{-1}$ $Na_2SO_4$ solution.

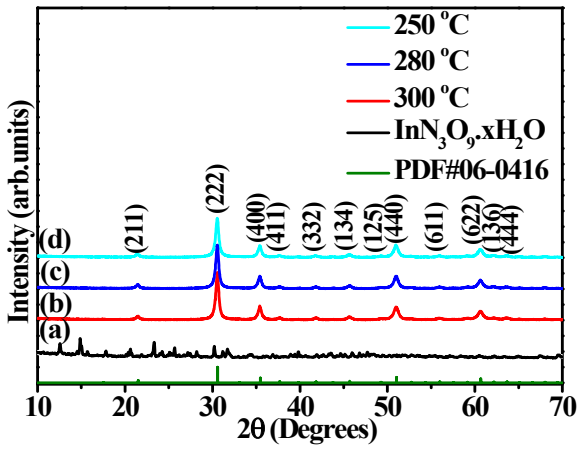


**Figure S3.** XRD patterns of $InN_3O_9 \cdot xH_2O$ (a) and $InN_3O_9 \cdot xH_2O$ calcined at 250 °C (b), 280 °C (c), and 300 °C (d). XRD analysis confirmed that calcination at 250 °C, 280 °C, and 300 °C for 4 hours consistently produced pure $In_2O_3$, as no diffraction peaks corresponding to indium nitrate were observed.

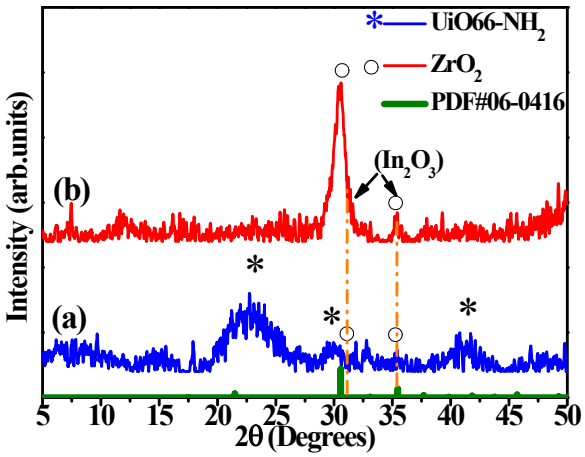


| Temperature (°C) | Products |
|---|---|
| 250 | UiO66-$NH_2$@$In_2O_3$ |
| 300 | UiO66-$NH_2$($ZrO_2$)/$In_2O_3$ |
| 350 | $ZrO_2$/$In_2O_3$ |

**Figure S4.** XRD patterns of UiO66-$NH_2$@$In^{3+}$ calcined at 300 °C (a) and 350 °C (b). Increasing the calcination temperature to 300 °C resulted in significantly weakened XRD diffraction peaks, though they remained assignable to UiO66-$NH_2$, indicating partial structural collapse (**Figures S4a**). At 350 °C, the XRD peaks corresponding to UiO66-$NH_2$ disappeared entirely, and only $ZrO_2$ and $In_2O_3$ diffraction peaks were observed, signaling complete framework decomposition. Specifically, the main diffraction peaks of $In_2O_3$ overlap with the peaks of $ZrO_2$ at around 30° and 35° (2θ), which makes it difficult to distinguish the $In_2O_3$ phase in the XRD pattern. The standard XRD pattern of $In_2O_3$ is for reference (PDF#06-0416). To provide a clearer view of the phase conversion of UiO66-$NH_2$@$In^{3+}$, the bottom of Figure S4 provides a detailed description of the product transformation as the calcination temperature increases from 250°C to 350°C. Initially, the product is UiO66-$NH_2$@$In_2O_3$ (250°C), which gradually transitions into a partially collapsed structure, UiO66-$NH_2$($ZrO_2$)/$In_2O_3$ (300°C). Ultimately, the structure fully collapses, resulting in a $ZrO_2$/$In_2O_3$ composite (350°C).

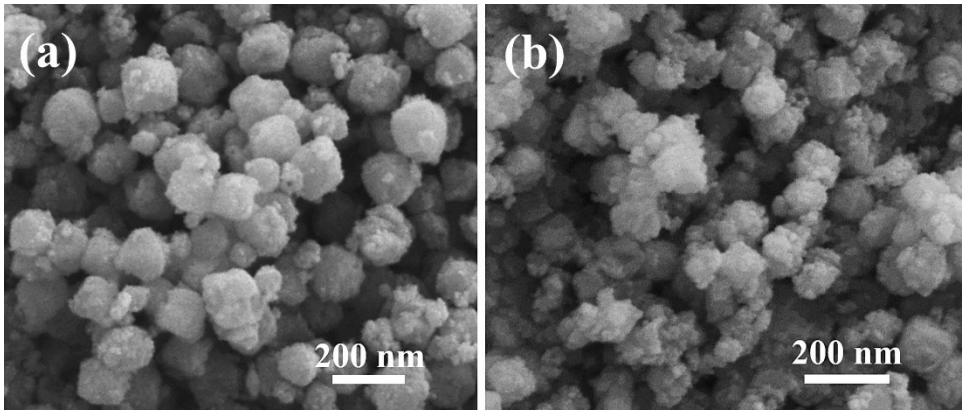


**Figure S5.** SEM images of UiO66-$NH_2$@$In^{3+}$ calcined at 300 °C (a) and 350 °C (b).

SEM analysis revealed that samples calcined at 300 °C exhibited partially collapsed structures with traces of octahedral morphology and the emergence of numerous nanoparticles (**Figures S5a**). At 350 °C, the structure collapsed entirely, leaving only aggregated nanoparticles (**Figures S5b**).

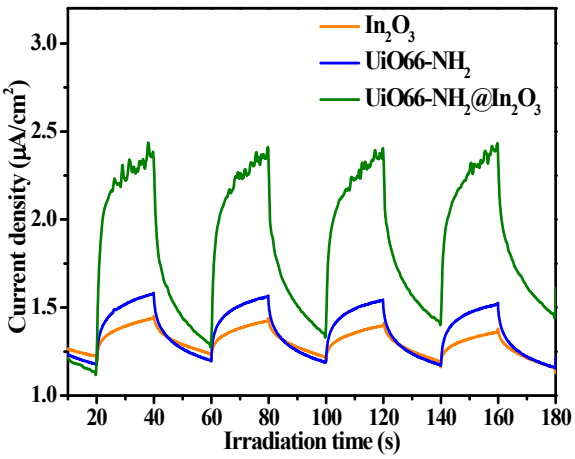


**Figure S6.** Photoelectrochemical measurements of UiO66-$NH_2$, $In_2O_3$, and UiO66-$NH_2$@$In_2O_3$ confirm enhanced photocatalytic activity, as evidenced by the significantly higher photocurrent observed for UiO66-$NH_2$@$In_2O_3$.